JOURNAL OF GEOPHYSICAL RESEARCH, VOL. 103, NO. C11, PAGES 24,573–24,583, OCTOBER 15, 1998

Slow oceanic teleconnections linking the Antarctic Circumpolar Wave with the tropical El Niño–Southern Oscillation

Ray G. Peterson and Warren B. White

Scripps Institution of Oceanography, University of California, San Diego, La Jolla

Abstract. A case study for the period 1982–1994 shows that a major source for the Antarctic Circumpolar Wave is in the western subtropical South Pacific, where interannual anomalies in sea surface temperature (SST) and precipitable water (PrWat) form. Once established, these interannual anomalies, in tandem with anomalies in sea level pressure (SLP), move south toward the Southern Ocean. The system then migrates east around the globe through a combination of oceanic advection with the Antarctic Circumpolar Current and ocean-atmosphere coupling. The coincidence of interannual anomalies in SST, SLP, and PrWat indicates the extratropical ocean and atmosphere are tightly linked on these timescales. Large portions of the interannual SST anomalies branch advectively northward into the South Atlantic and Indian Oceans, ultimately reaching the tropics in each basin some 6–8 years after appearing in the low-latitude Pacific. This constitutes a slow, oceanic teleconnection that is unique in climate dynamics, made possible by the continuity of Earth's oceans via the Southern Ocean. In the tropical Indian Ocean these interannual anomalies move east and arrive at the Indo-Pacific transition in advance of the trans-Pacific propagation of the respective El Niño–Southern Oscillation (ENSO) phases. The interannual SST and PrWat anomalies that appear in the subtropical South Pacific are directly linked with the ENSO cycle on the equator through anomalous vertical convection and a regional overturning cell in the troposphere, the same cell that initiates fast planetary waves in the atmosphere that carry ENSO signals around the southern hemisphere on much shorter timescales.

1. Introduction

The El Niño–Southern Oscillation (ENSO) contributes much to variations in global climate in both the atmosphere and ocean [*Bjerknes*, 1969; *Wooster and Fluharty*, 1985; *Karoly*, 1989; *Philander*, 1990; *Trenberth*, 1991; *Tribbia*, 1991; *Rasmusson*, 1991; *Tourre and White*, 1995, 1997]. In recent decades, ENSO has typically occurred over periods ranging from 3–5 years. Dominant signatures of ENSO are found in sea surface temperature (SST) and atmospheric vertical convection in the equatorial Pacific Ocean, with warm SST anomalies driving anomalous upward convection. The latter generates anomalous meridional overturning cells in the western Pacific tropical atmosphere (regional Hadley cells) [*Rasmusson and Mo*, 1993], which at their poleward termini (20°–30° latitude) initiate trains of quasi-stationary planetary waves. These waves transmit ENSO signals from the low-latitude Pacific throughout the middle and high latitudes over a few days or weeks [*Sardeshmukh and Hoskins*, 1988]; this entire process has been termed atmospheric teleconnection [*Bjerknes*, 1969].

ENSO timescale climatic signals have been detected in high southern latitudes [*Fletcher et al.*, 1982; *van Loon and Shea*, 1985, 1987; *Carleton*, 1988; *Savage et al.*, 1988; *Smith and Stearns*, 1993; *Simmonds and Jacka*, 1995], and eastward propagation of interannual anomalies in the ice field around Antarctica has been observed on ENSO scales [*Zwally et al.*, 1983; *Murphy et al.*, 1995], though connections with other propagating anomalies were not known. Recently, *White and Peterson* [1996] (hereinafter referred to as WP96) and *Jacobs and Mitchell* [1996] found anomalies in the ocean and atmosphere propagating around the southern hemisphere on ENSO timescales. Using atmospheric sea level pressure (SLP), surface winds, sea surface temperature (SST), and sea ice extent data, WP96 identified a coupled set of wavenumber-2 climatic anomalies propagating east around the Southern Ocean with the Antarctic Circumpolar Current (ACC) at average speeds of ~8 cm s^{-1}, thus requiring 8–10 years for individual phases of the wave train to circle the globe. This Antarctic Circumpolar Wave (ACW) is also found in changes in the height of the sea surface as measured by satellite altimeters [*Jacobs and Mitchell*, 1996], with the changes correlating directly with those in SST. WP96 noted that SST anomalies appeared to enter the ACW from lower latitudes in the western South Pacific and speculated that there might be an atmospheric teleconnection between El Niño activity in the equatorial Pacific and the ACW.

Models of the ACW show there must be a coupling between the ocean and atmosphere for this interannual phenomenon to exist. *Qiu and Jin* [1997] used a wind-driven, two-layer, quasi-geostrophic model of the ocean in a zonal channel coupled with an equivalent-barotropic atmosphere assumed to be in equilibrium with the ocean to find that a coupled instability of the system may account for the generation of the ACW. They also analyzed global wind data to conclude that the ACW is not remotely forced by tropical El Niño activity through a meridional atmospheric teleconnection. Using a quasi-stationary vorticity model of the lower atmosphere and a heat budget model of the upper ocean, *White et al.* [1998] found that in the absence of coupling, the ACC advects SST anomalies from initial conditions to the east at speeds slower than observed

Paper number 98JC01947.
0148-0227/98/98JC-01947$09.00

(~4–6 cm s^{-1}), with the anomalies becoming insignificant after 6–8 years; with coupling, speeds of the model ACW became close to those observed, with the maintenance of the coupled wave occurring through a balance between anomalous meridional Ekman heat advection and exchange of heat with the atmosphere. L. D. Talley (Simple coupled mid-latitude models for decadal climate modes, submitted to *Journal of Physical Oceanography*, 1998) also employed a simple vorticity model of the atmosphere, together with various choices for the upper ocean velocity, to find that in addition to the balance obtained by *White et al.* [1998], another possible balance can be between zonal advection in the ocean and heat exchange with an equivalent-barotropic atmosphere. A Max-Planck Institute coupled general circulation model was run for 180 years of model time by *Christoph et al.* [1998], who found dominating wavenumber-3 patterns in atmospheric, oceanic, and sea ice variables. Unlike observations, their model showed little or no eastward propagation of the atmospheric anomalies, while the SST and ice extent anomalies propagated at only 4–6 cm s^{-1}, the same as the speeds obtained by *White et al.* [1998] for the uncoupled case. *Christoph et al.* [1998] hypothesized that their modeled SST anomalies were the result of those advected anomalies interacting with a spatially fixed atmospheric forcing pattern, in which case there was no direct air-sea coupling in the sense of the observed ACW.

Features not yet seen in models but which were noted by WP96 are that SST anomalies appear to feed into the ACW from a more northerly source in the western South Pacific and that during their eastward migration around the Southern Ocean, portions of the anomalies subsequently spread north into the South Atlantic and South Indian Oceans. Here we identify the western subtropical South Pacific (WSSP) (roughly 20°–30°S, 150°E–150°W) as a low-latitude source for interannual SST signals in the ACW, at least for the period of 1982–1994. They develop in response to ENSO along the equator, and together with anomalies in precipitable water (PrWat), they migrate south in the western South Pacific in tandem with interannual anomalies in SLP. We find the subsequent hemispheric propagation of these Pacific ENSO signals to generally follow the path of the ACC, but in other domains their motions do not necessarily correspond to paths taken by oceanic fluid parcels, which must be due to feedbacks within the coupled air-sea system. Portions of these signals eventually end up in the tropical South Atlantic and Indian Oceans. Thus ENSO signals from the Pacific Ocean, in addition to being transmitted around the globe by fast planetary waves in the atmosphere [*Karoly*, 1989; *Rasmusson*, 1991], also propagate throughout the southern hemisphere via a much slower oceanic process. This is facilitated by the circumpolar continuity of the Southern Ocean. The initial generation of these slowly propagating interannual SST anomalies derives from an anomalous, regional Hadley cell in the troposphere [*Rasmusson and Mo*, 1993] that links the WSSP directly with ENSO on the equator, the same cell that is thought to initiate fast atmospheric planetary waves in the upper troposphere.

2. Data and Methods

Two data sets used here span the 13-year period of 1982–1994: (1) monthly mean atmospheric parameters on a 2.5° grid as provided by the National Centers for Environmental Prediction (NCEP) and the National Center for Atmospheric Research (NCAR) [*Kalnay et al.*, 1996] and (2) monthly mean SSTs on a 2° grid derived from a combination of in situ and satellite radiometer measurements [*Reynolds*, 1988; *Reynolds and Marisco*, 1993; *Reynolds and Smith*, 1994]. We also use monthly mean atmospheric parameters on a 1.875° grid over the 10-year period of 1985–1994 as produced by the European Centre for Medium-Range Weather Forecasts [*ECMWF*, 1993]. The two models used to produce the atmospheric data are very similar, and they are also not completely independent of the SST data set in that they each use SST as a surface boundary condition. It is not known to what extent the model results are biased by this, but preliminary comparisons of the ECMWF model winds and moisture with observations from the midlatitude and high-latitude southern hemisphere have shown good overall agreement [*Sinclair and Cong*, 1992; *Bromwich et al.*, 1995; *Genthon and Braun*, 1995]. Two precipitation variables are available in the NCEP/NCAR data set: precipitation rate (total and convective) and PrWat. The latter is the total mass of water per unit horizontal area that would be obtained if all the water vapor in the air column were condensed out. We have chosen to use PrWat because it is determined partly from observational data, whereas precipitation rate is derived solely from model fields. Initially, we worked with both and found them to exhibit nearly identical patterns of interannual anomalies. For a high midlatitude region, *Ebert et al.* [1996] found that numerical weather prediction routinely provides superior fields of precipitation than do algorithms using parameters measured by satellite. Over interannual periods and large spatial scales the NCEP/NCAR, ECMWF, and Reynolds products are expected to provide satisfactory renditions of actual variations.

As in WP96, time series of monthly anomalies in each parameter at each grid point are determined relative to the applicable record-length monthly mean values, thus removing the long-term mean annual and semiannual cycles. To further suppress relatively short-period and quasi-biennial signals [*Trenberth*, 1975] and to remove long-term trends, all time series are then band-passed with a filter [*Kaylor*, 1977] having a 3–7 year admittance window. Data losses at the ends of the time series due to filtering are avoided by extending the records on each end by a filter width using a maximum-entropy method that retains the spectral composition of the original series (J. Bottero, Oregon State University, personal communication, 1994). The filtered time series are further smoothed in space with three passes of a 1-1-4-1-1 weighted filter in each the zonal and meridional directions. The sign convention used here is that positive anomalies denote higher-than-normal SST, SLP, PrWat, northward and eastward winds, divergence of wind, and upward heat flux.

A fundamental aspect of ENSO is its seasonality [*van Loon and Shea*, 1985; *Karoly*, 1989; *Rasmusson*, 1991], so it is common practice to consider phases of individual ENSO cycles for specific seasons or to form composites from particular phases of two or more ENSO cycles, also for specific seasons. We do not follow that methodology here but, instead, filter the data so we can perform extended empirical orthogonal function (EEOF) analyses [*Graham et al.*, 1987; *Preisendorfer*, 1988] in consistent ways on each the SST, SLP, and PrWat anomalies and provide a consistent bridge between the results of WP96 and the southern hemisphere as a whole. In WP96, two-dimensional autospectra, in wavenumber-frequency space, of the unfiltered monthly anomalies of SST and SLP along 56°S and in sea ice extent along meridians showed that the filtering isolates the most important interannual variability occurring in

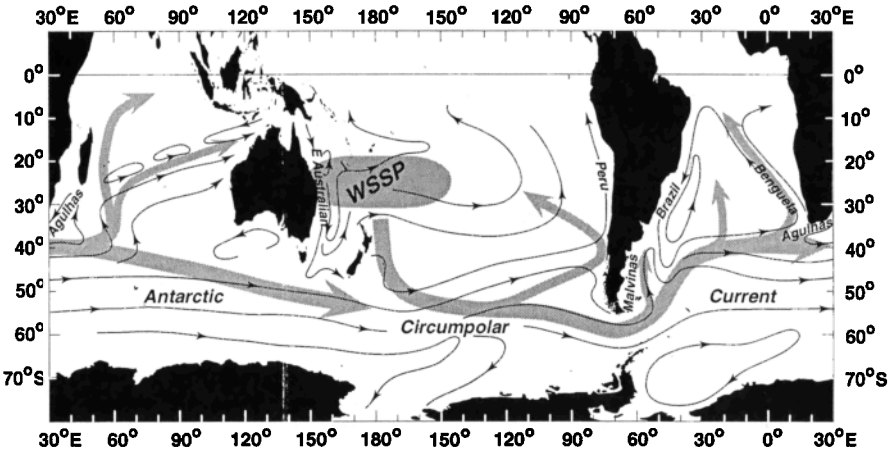

Figure 1. Schematic representation of the principal off-equatorial spreading routes (shaded lines) of interannual anomalies in sea surface temperature from the source region in the western subtropical South Pacific (WSSP) (shaded oval). Solid lines show the mean geostrophic circulation patterns at the sea surface as depicted by *Wyrtki* [1971] for the South Indian Ocean, *Reid* [1986] for the South Pacific Ocean, and *Reid* [1989] for the South Atlantic Ocean.

all the records, about 4 years in period locally with wavelengths of about half the circumpolar distance. Though seasonality is important to atmospheric teleconnections, there are net effects in the coupled atmosphere-ocean system that persist, and over interannual timescales these have climatically important propagational patterns around the southern hemisphere.

3. Slow Hemispheric Propagation of ENSO-Scale Anomalies

The spreading patterns of ENSO-scale SST anomalies are well known for the equatorial Pacific waveguide, and the work of WP96 has shown how SST anomalies on these timescales propagate around the Southern Ocean. Here we investigate the connections between these two regimes and how ENSO-scale anomalies subsequently spread northward into the South Atlantic and Indian Oceans. We provide as reference in Figure 1 a schematic summary of the most important nonequatorial propagational paths of ENSO-scale SST anomalies around the southern hemisphere. Also shown are the mean patterns of geostrophic currents at the sea surface, which are based on the analyses of *Wyrtki* [1971] (South Indian Ocean), *Reid* [1986] (South Pacific Ocean), and *Reid* [1989] (South Atlantic Ocean). The propagational paths of SST anomalies and the directions of surface currents coincide in most areas, but there are discrepancies in others, particularly in the western South Pacific, that indicate the signal propagation cannot be attributed to geostrophic advection alone but that mechanisms which couple the air-sea system must be important. This is a subject of ongoing work.

3.1. Extended Empirical Orthogonal Functions

An EEOF analysis of interannual SST anomalies was presented by WP96 for the latitude band 30°–80°S. The first mode accounted for 51% of the total variance and clearly showed how the ACW propagates east with the circumpolar flow, while also indicating that the ACW communicates with the subtropical regions farther north. Here the analysis is extended to encompass the entire southern hemisphere ocean, 0°–80°S, for SST, SLP, and PrWat (Plate 1). The lag sequences in Plate 1 span 4 years to capture roughly a half cycle of the two-wavelength ACW. The lag sequences here are computed over a longer time interval (13 years) than that used by WP96 (10 years), so there are differences in detail, but the overall patterns are the same.

For brevity, we qualitatively associate the mathematical EEOF loadings or weightings with physical anomalies. The patterns so revealed by the EEOFs are simplifications of those described by the actual interannual anomalies and may be considered the canonical ways in which the anomalies propagated spatially through our time window. In the next section we show sequences of the actual filtered anomalies which allows for the tracking of individual features and for seeing that the patterns vary from cycle to cycle, much as ENSO patterns along the equatorial Pacific vary between cycles [*Rasmusson*, 1991]. In the following paragraphs we describe in some detail the evolution and propagation of cold anomalies; the descriptions also apply to warm anomalies with a phase shift of about 2 years. We then briefly describe the EEOFs for SLP and PrWat which suggest a strong coupling between the atmosphere and ocean.

In Plate 1 the SST anomalies that WP96 observed to move into the ACW from the lower-latitude South Pacific appear to originate in the WSSP. In the first SST lag (month 0) a cold anomaly is starting to form in that area, at the same time as a warm feature is moving east along the equator from the Indonesian domain. Conversely, 2 years later (month 24) a warm anomaly just begins to appear in the WSSP while cold SSTs are moving east from the Indonesian area. The significance of these relations involves an anomalous atmospheric convection cell linking the equatorial ENSO cycle with the WSSP, which is explored more fully in section 4.

Initially, the cold feature in the WSSP in month 0 grows more in the zonal direction than in the meridional, facilitated by the upper level circulation (Figure 1), and it subsequently coalesces with two other cold features. The first is with a cold anomaly spreading from the Indian Ocean into the Pacific around both the north and south sides of Australia, while the second is farther east where the growing cold anomaly coalesces with another that has moved from the ACC north into

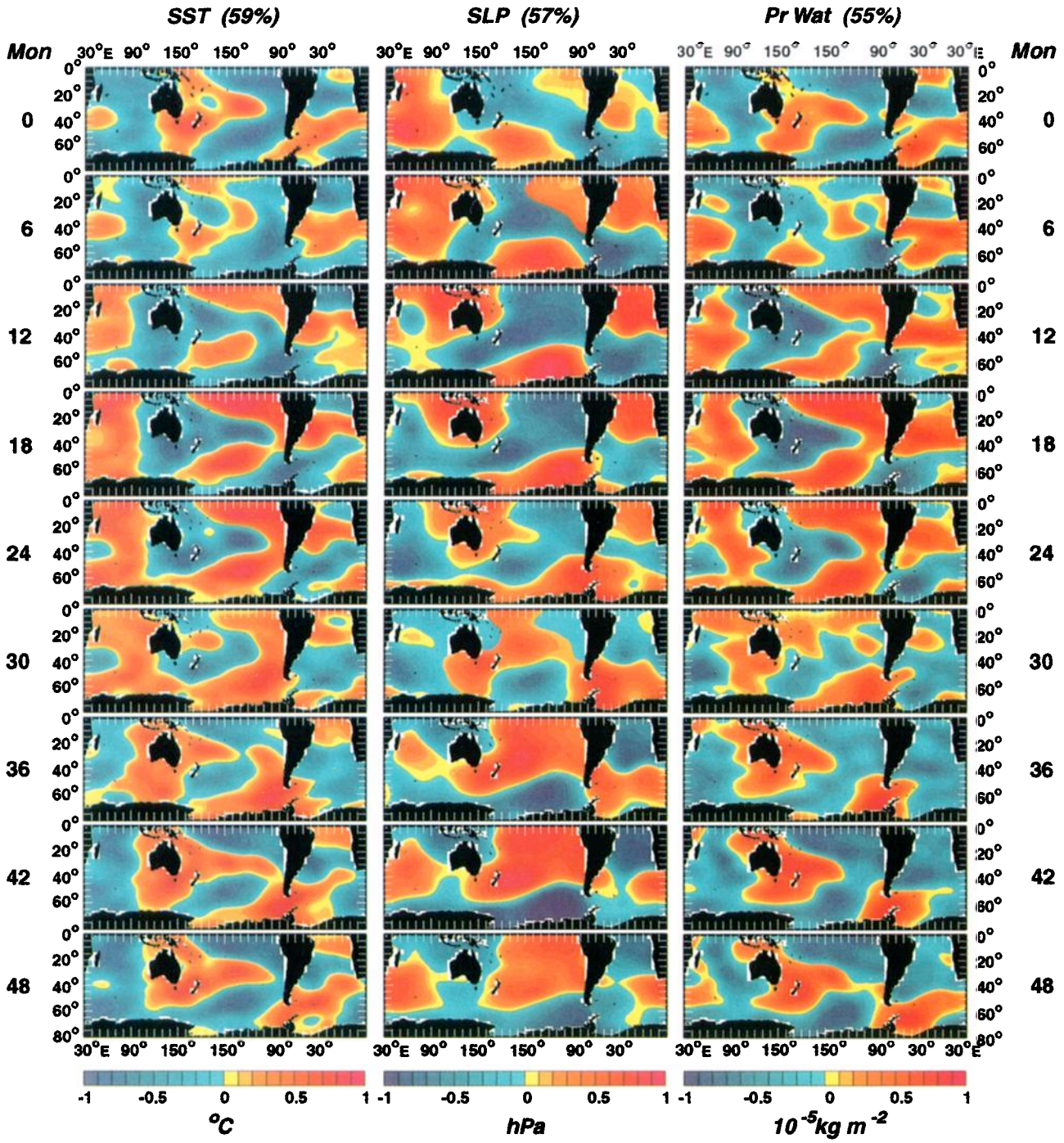

Plate 1. Lag sequences of the dominant modes of extended empirical orthogonal function (EEOF) analyses on interannual anomalies of (left) sea surface temperature (SST), (middle) atmospheric sea level pressure (SLP), and (right) tropospheric precipitable water (PrWat). Percentages given at top are the amounts of total variances in the band-passed data accounted for by the EEOFs over the 13-year period 1982–1994. The EEOFs are computed from the covariances of state vectors for standardized interannual anomalies, yielding estimates with equal variances over the fields. This allows propagation to be seen unbiased by regions of strong and weak variance.

the Peru Current and then west in the subtropics. The continuity of this "reverse-c" shape, seen in month 12, is broken by month 18 when the remainder of the southern cold anomaly moves east into Drake Passage and the South Atlantic. The cold anomaly in the WSSP then drifts mainly south, and after passing New Zealand by month 30 it moves southeast and into the Southern Ocean by month 48, where it replaces a similar feature that was there in month 0.

Following the earlier cold feature in the south central South Pacific in month 0, part of it recirculates in the South Pacific while the rest moves into the South Atlantic. Once in the South Atlantic, it extends across the basin between months 12 and 18,

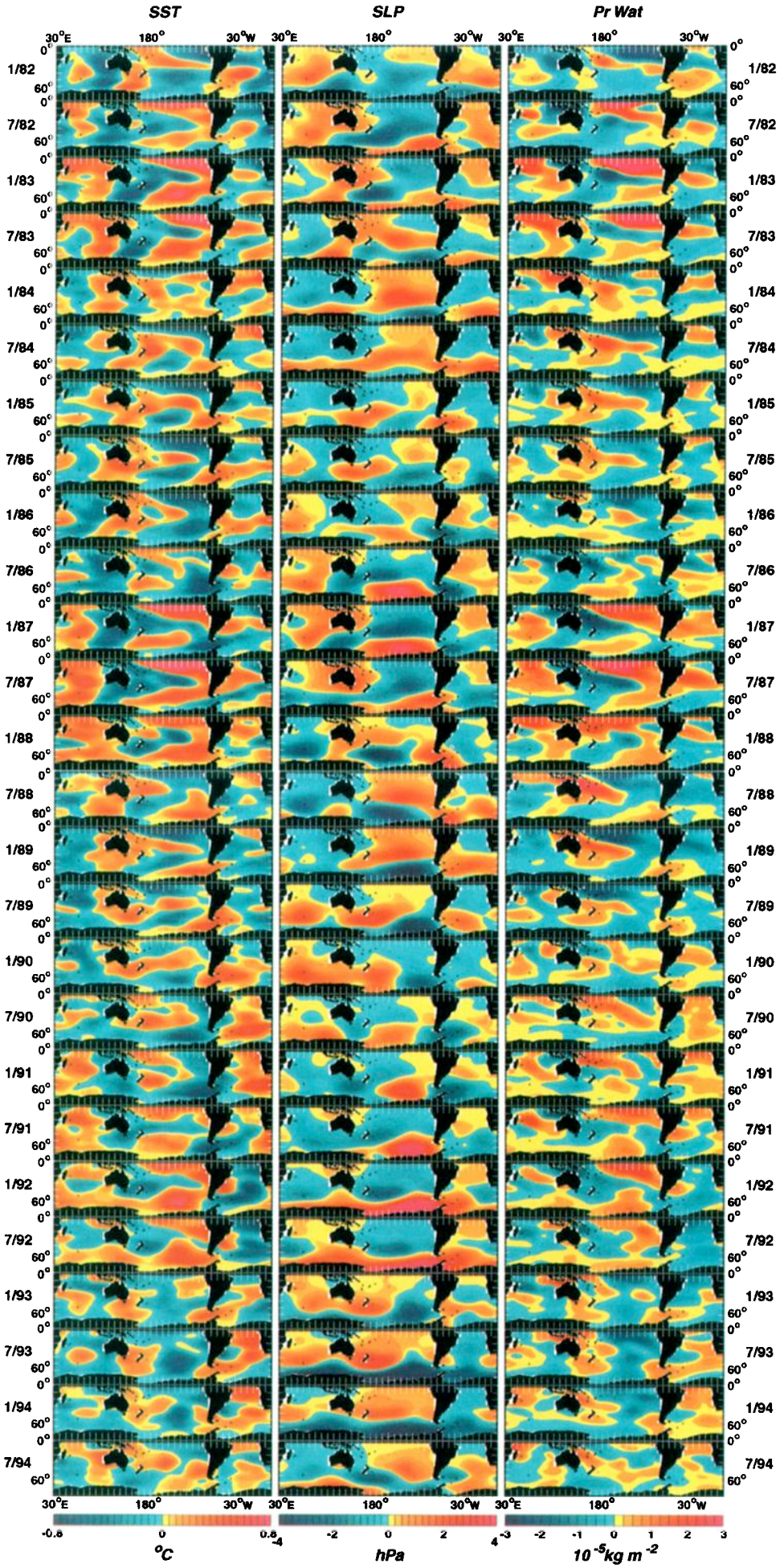
SST
SLP
Pr Wat
30°E
180°
30°W
0°
60°
1/82
7/82
1/83
7/83
1/84
7/84
1/85
7/85
1/86
7/86
1/87
7/87
1/88
7/88
1/89
7/89
1/90
7/90
1/91
7/91
1/92
7/92
1/93
7/93
1/94
7/94
-0.6
0
0.6
°C
-4
-2
0
2
4
hPa
-3
-2
-1
0
1
2
3
10 -5kg m -2

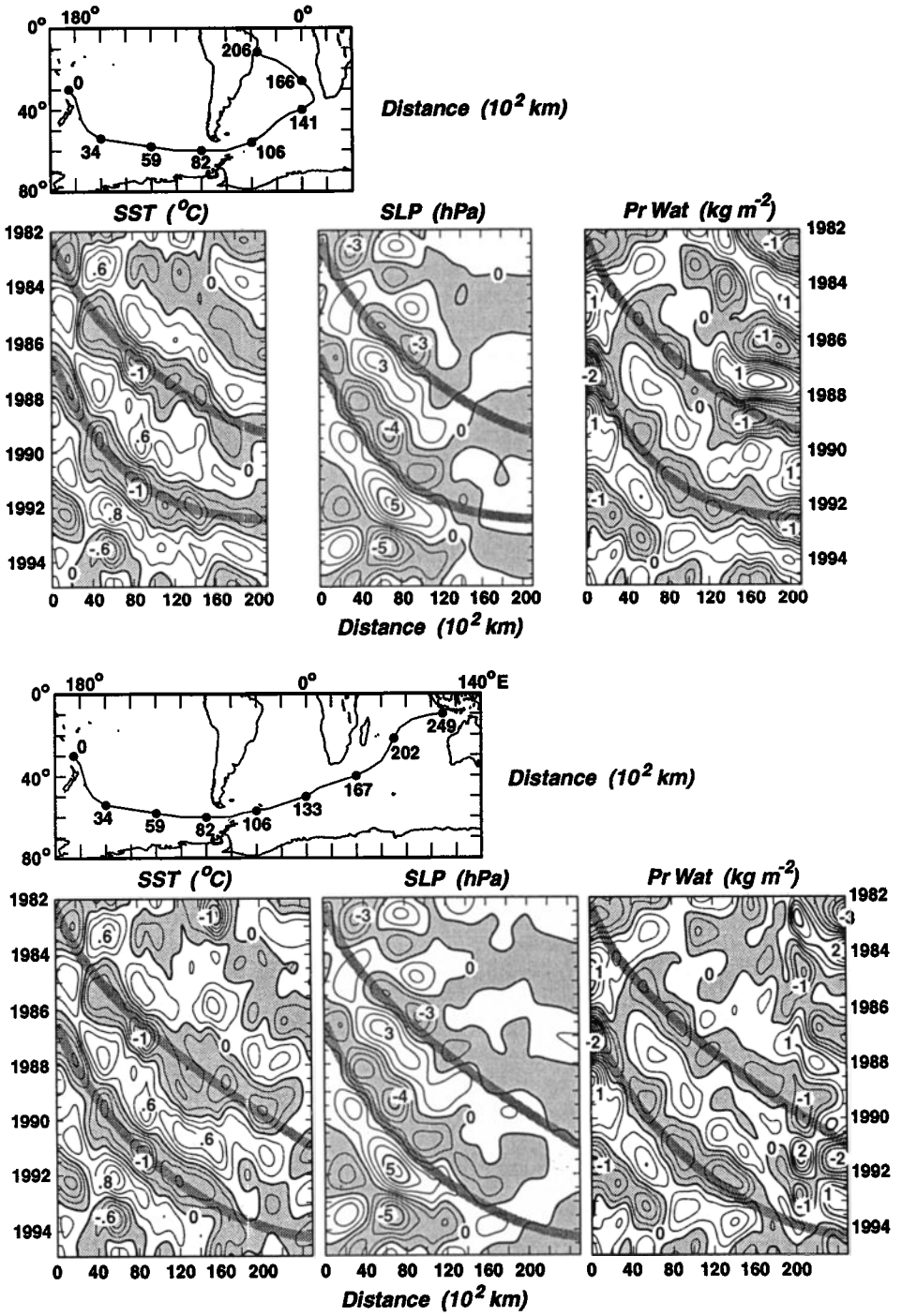

Figure 2. Time-distance propagation along indicated routes of El Niño–Southern Oscillation (ENSO) scale (3–7 year) anomalies in sea surface temperature (SST), atmospheric sea level pressure (SLP), and tropospheric precipitable water (PrWat). Negative anomalies are shaded. The curved lines for each route are synchronous in time and space.

Plate 2. (opposite) Time sequences of interannual anomalies in (left) sea surface temperature (SST), (middle) atmospheric sea level pressure (SLP), and (right) tropospheric precipitable water (PrWat) at 6-month intervals for the period 1982–1994 after being passed through a filter having a 3–7 year admittance window.

illustrated by the warm anomalies appearing there in late 1983 and early 1988 and cold anomalies appearing in late 1985 and late 1989. The lateral growths of these anomalies are consistent with changes in the volumes of Subtropical Mode Water (temperatures of 14°–20°C) calculated along a line from New Zealand northward to Fiji and which were attributed to ENSO

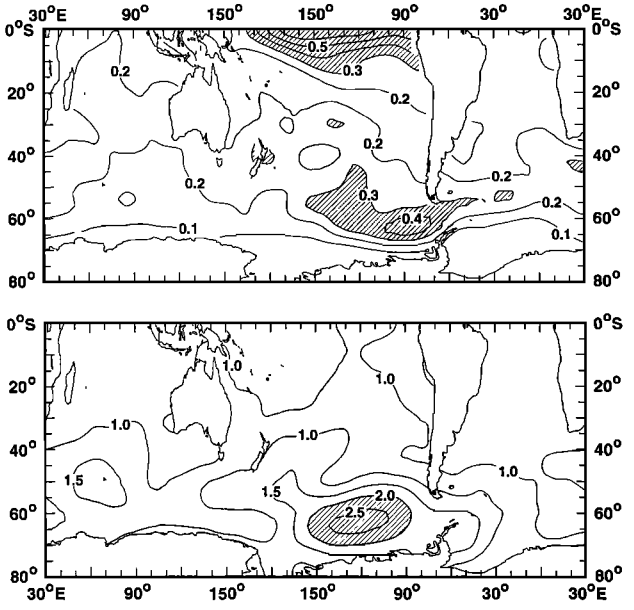

Figure 3. Root-mean-square (RMS) variability of (top) sea surface temperature (SST) in degrees Celsius and (bottom) atmospheric sea level pressure (SLP) in hectopascals for the 13-year period 1982–1994 after the original monthly mean data were passed through a filter having a 3–7 year admittance window. Note the increasing values of each from the western subtropical South Pacific toward the Southern Ocean and Drake Passage.

variability on the equator [*Sprintall and Roemmich*, 1995]. Subsequent motions of these anomalies are much like those described by the EEOFs in Plate 1. The regularity of how they consequently move into the Southern Ocean and then back north into the eastern Pacific, Atlantic, and Indian Oceans is demonstrated by the time-distance diagrams in Figure 2. The paths are selected to follow the major currents as much as possible (Figure 1), but because of the large spatial scales and coherence, other paths into the South Atlantic and Indian Oceans could be selected to show the propagation just as well. Among the slowest moving SST signals are those propagating south from the WSSP, at about 4–5 cm s^{-1}. Once in the Southern Ocean, they translate eastward at about 8 cm s^{-1}, and after turning north into the Atlantic and Indian Oceans they appear to accelerate further, but this is partly an artifact of the large spatial scales occupied by the propagating anomalies in relation to the selected paths.

Figure 2 shows that the interannual anomalies in SST and PrWat maintain a strong inphase relationship everywhere, as seen with the EEOFs. This may be an artifact of the model, but there is probably some validity in it. Figure 2 also shows that interannual SLP anomalies lead similar phases of SST anomalies by 6–12 months in the western South Pacific and, more consistently, by about a year within the Southern Ocean as observed by WP96. SST and SLP tend toward decorrelation in the South Atlantic and South Indian Oceans where the interannual variability of SLP is weak (Figure 3).

Conspicuous features in Figure 3 are the strong RMS variations in both SST and SLP within and west of Drake Passage. For SST, RMS variability in the region of the Southern Ocean centered at 80°–90°W approaches 70% of the variability seen in the equatorial Pacific, and for SLP the Southern Ocean variability centered near 120°W is by far the greatest seen anywhere in the southern hemisphere. These features are evident as well in Plate 2 and Figure 2, in that interannual SST and SLP anomalies intensify markedly as they approach Drake Passage from the west. The greatest Southern Ocean RMS variability in SST lies east of that in SLP (Figure 3), which implies a delayed response of the ocean to the atmosphere, by about a year. This is consistent with the phase relations between SST and SLP and with the propagation speed of the ACW being about 40° yr^{-1}. Furthermore, the RMS values in each parameter increase from the WSSP south and east toward Drake Passage, indicating that the feedback mechanisms responsible for making the SST anomalies propagate across the surface currents in the western Pacific also serve to strengthen the anomalies.

4. Low-Latitude Development of SST Anomalies

The warm phase of ENSO is characterized by anomalous upward motions of air over the equatorial Pacific, matched by anomalous divergence of wind in the upper troposphere. This anomalous divergence must be balanced by anomalous convergences and subsidence elsewhere in the upper troposphere, and this has often been thought to occur uniformly over the western and central Pacific. However, observational evidence now shows that this compensation tends to be localized [*Sardeshmukh and Hoskins*, 1988] and can be described in terms of a regional Hadley cell with anomalous meridional circulations [*Rasmusson*, 1991]; these provide extraequatorial vorticity sources for the forcing of tropospheric planetary waves that communicate ENSO signals to higher latitudes. In the South Pacific the poleward limb of the seasonally dependent regional Hadley cell is centered over an area north of New Zealand [*Rasmusson*, 1991].

Inspection of Plates 1 and 2 shows that SST anomalies appear in the WSSP after anomalies of opposite sign have become established in the Indonesian area and begin to move east. Anomalies in the WSSP grow rapidly as those of the opposite sign pass directly to the north along the equator. This sequence occurs during both phases of ENSO, and it produces net effects that persist through the strong seasonality of ENSO.

Atmospheric data from the ECMWF model, passed through our 3–7 year filter, reveal the regional Hadley cell and further implicate it as driving the interannual SST anomalies in the WSSP. In Figure 4a the zonal convective Walker cell along the equator in the Pacific is clear in the strong negative correlations in zonal wind anomalies between the upper and lower troposphere, the greatest vertical shears occurring directly north of the WSSP. Also occurring there, but offset from the equator and at slightly reduced amplitudes, are negative correlations in meridional wind anomalies between the upper and lower troposphere (Figure 4b). These strongly negative correlations, in both the zonal and meridional wind anomalies, are coupled through anomalous equatorial convection. This, in turn, is manifested in anomalous lower and upper level wind divergences, both of which have maximal values of RMS variability on the equator directly north of New Zealand (not shown). These maximal RMS variations, along with the world's strongest negative correlations between lower and upper tropospheric zonal winds, occur in the region often referred to as Niño 4 (5°N–5°S, 160°E–150°W, e.g., *Trenberth and Hoar* [1996]). Here we use the same region, but for 160°E–160°W, and compute the covariance of divergence anomalies there

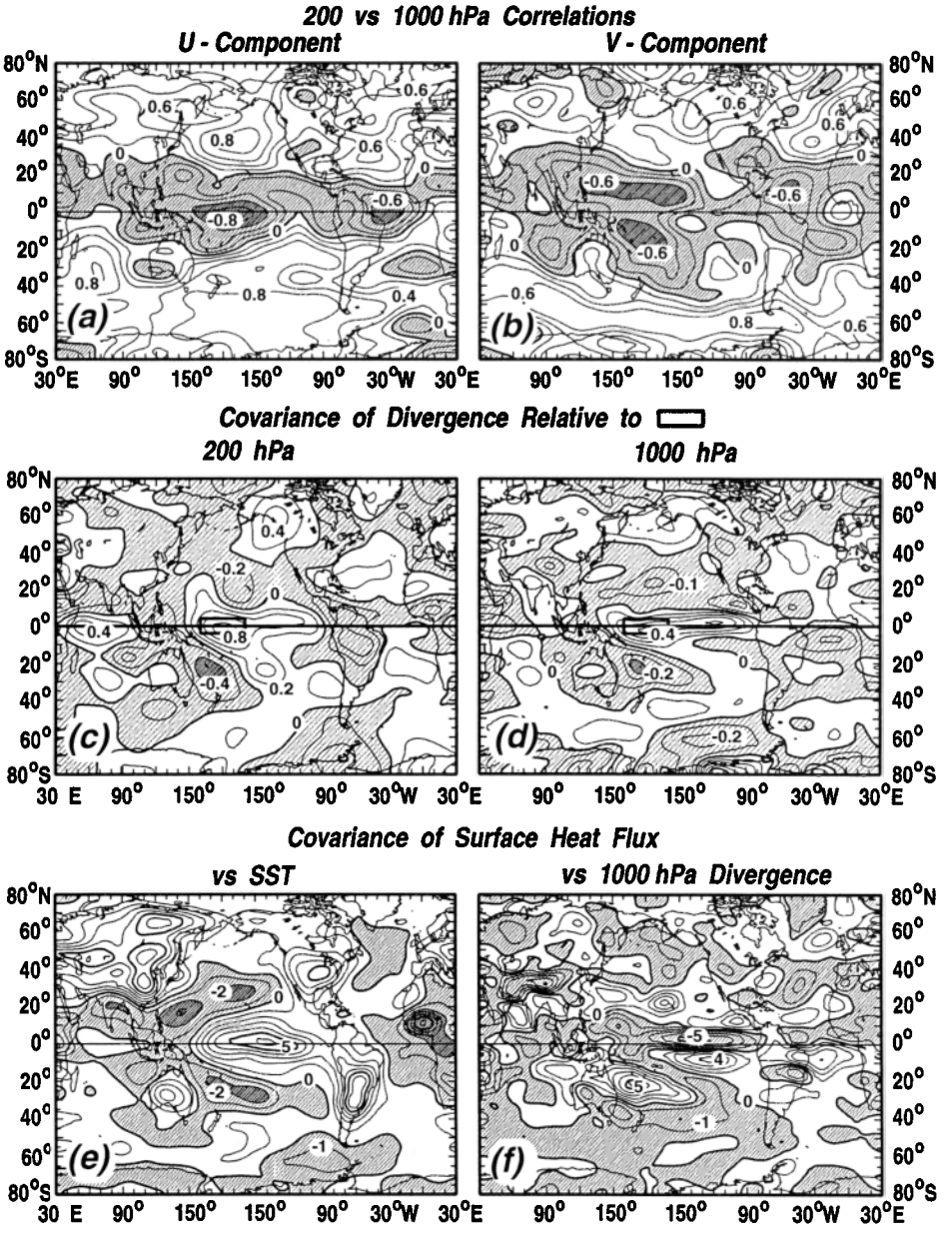

Figure 4. Correlations of ENSO-scale wind anomalies between 200 (hPa) (or millibars) and 1000 hPa for (a) eastward U and (b) northward V components. Covariances of ENSO-scale wind divergence anomalies, calculated at every point in the field relative to the rectangle over the equator north of New Zealand, at (c) 200 and (d) 1000 hPa. Units are 10^{-12} s^{-2}. Covariances of ENSO-scale anomalies of net heat flux at the sea surface (upward is positive) versus anomalies in (e) sea surface temperature (SST) and (f) wind divergence at 1000 hPa. Units are °C W s m^{-2} in Figure 4e and hPa W s m^{-3} in Figure 4f. The atmospheric parameters are from the European Centre for Medium-Range Weather Forecasts model; all fields span 1985–1994.

with those everywhere else in the field, at both levels (Figures 4c and 4d). At each level, strong negative covariances occur over the WSSP, consistent with the existence of a regional Hadley cell responding to anomalous equatorial convection.

Exchanges of heat energy between the ocean and atmosphere are often thought of in terms of temperature advection by ocean currents, such as when the warm Gulf Stream provides heat to the atmosphere or the cold California Current draws heat out of the overlying air. Such positive correlations between anomalies in SST and surface heat flux act to dampen SST anomalies. These correlations occur as well on interannual timescales along the equator, where, for example, the advection of abnormally warm SSTs by the transient flows provide the heat necessary for anomalous upward convection in the atmosphere. This direct relationship is seen in Figure 4e over the central and eastern equatorial Pacific, but, in each hemisphere a poleward band occurs where this relationship is reversed, indicating regions where SST anomalies intensify in their respective directions instead of weakening. This includes the WSSP, where, additionally, there are strong positive covariances on ENSO timescales between anomalies in surface heat flux and divergence of surface winds (Figure 4f).

In combination, Figures 4a–4f demonstrate that when sea surface temperatures are anomalously high at the equator

north of New Zealand, anomalous ascending motion exists in the atmosphere there. This is balanced, in part, by anomalous descending motion over the WSSP, yielding positive surface divergence anomalies and strong upward heat flux, thus leading to a cooling of the ocean. Conversely, when equatorial SSTs are abnormally low within Niño-4, the anomalous vertical motions in the atmosphere change directions and the WSSP warms. This matches well with the patterns seen in Plates 1 and 2. Interannual SST anomalies appearing in the WSSP are therefore linked directly to the equatorial ENSO cycle via a regional Hadley cell in the atmosphere. Such a cell also appears to exist in the northern hemisphere at similar longitudes, though weaker than in the southern, and how this may influence SST anomalies there is a subject of ongoing work. With regard to the southern hemisphere, it is evident that the same mechanism that initiates the fast atmospheric teleconnections which, in turn, transmit ENSO signals around the globe also initiates a slow, coupled oceanic-atmospheric teleconnection that transmits SST, SLP, and PrWat anomalies all around the southern hemisphere.

5. Conclusions

This case study demonstrates that the ACW has a major source in the western subtropical South Pacific Ocean, where local interannual SST anomalies are driven by ENSO activity directly north on the equator through the influence of an intervening regional Hadley cell. Subsequently, these ENSO-scale SST anomalies, together with those in PrWat, propagate southward into the Southern Ocean in tandem with SLP anomalies. All these propagate around the southern hemisphere as the ACW through some combination of geostrophic oceanic advection and ocean-atmosphere coupling. The coincidence of SST, SLP, and PrWat indicates the ocean and atmosphere are inextricably linked, with SST having a significant influence upon the atmosphere in this extratropical domain. The zonal propagation of the ACW, together with its associated meridional propagation in all three oceans, allows ENSO in the tropical Pacific to influence ocean climate in the tropical Atlantic and Indian Oceans some 6–8 years later. This constitutes an oceanic teleconnection that is unique in climate dynamics, made possible by the continuity of Earth's oceans via the Southern Ocean.

The extent to which the ACW phenomenology described here is stable cannot be known from the relatively short data sets available. It is possible that the patterns we observe for the 1980s and early 1990s represent just one mode of interannual variability that could be modified or supplanted by other modes during other periods of time. Much longer observational data sets are required to address this. Nonetheless, the coupled system of interannual anomalies observed here does reveal potentially important climatic processes that warrant further study.

Acknowledgments. This work has been supported by the National Science Foundation, Division of Ocean Sciences (OCE-9633474). We thank Ted Walker for conducting the data analyses and helping to construct the figures.

References

Bjerknes, J., Atmospheric teleconnections from the equatorial Pacific, *Mon. Weather Rev.*, *97*, 163–172, 1969.

Bromwich, D. H., F. M. Robasky, R. I. Cullather, and M. L. Van Woert, The atmospheric hydrologic cycle over the Southern Ocean and Antarctica from operational numerical analyses, *Mon. Weather Rev.*, *123*, 3518–3538, 1995.

Carleton, A. M., Sea ice-atmosphere signal of the Southern Oscillation in the Weddell Sea, Antarctica, *J. Clim.*, *1*, 379–388, 1988.

Christoph, M., T. P. Barnett, and E. Roeckner, The Antarctic Circumpolar Wave in a coupled ocean-atmosphere GCM, *J. Clim.*, in press, 1998.

Cutler, A. N., and J. C. Swallow, Surface currents of the Indian Ocean (to 25°S, 100°E), *Rep. 187*, 7 pp., 36 plates, Inst. of Oceanogr. Sci., Wormley, England, 1984.

Ebert, E. E., M. J. Manton, P. A. Arkin, R. J. Allam, G. E. Holpin, and A. Gruber, Results from the GPCP Algorithm Intercomparison Programme, *Bull. Am. Meteorol. Soc.*, *77*, 2875–2887, 1996.

European Centre for Medium-Range Weather Forecasts (ECMWF), Description of the ECMWF/WCRP Level III—A global atmospheric data archive, technical attachment, Reading, England, 1993.

Fletcher, J. O., U. Radok, and R. Slutz, Climatic signals of the Antarctic Ocean, *J. Geophys. Res.*, *87*, 4269–4276, 1982.

Genthon, C., and A. Braun, ECMWF analyses and predictions of the surface climate of Greenland and Antarctica, *J. Clim.*, *8*, 2324–2332, 1995.

Graham, N. E., J. Michaelsen, and T. P. Barnett, An investigation of the El Niño–Southern Oscillation cycle with statistical models, 1, Predictor field characteristics, *J. Geophys. Res.*, *92*, 14,251–14,270, 1987.

Jacobs, G. A., and J. L. Mitchell, Ocean circulation variations associated with the Antarctic Circumpolar Wave, *Geophys. Res. Lett.*, *23*, 2947–2950, 1996.

Kalnay, E., The NCEP/NCAR 40-year reanalysis project, *Bull. Am. Meteorol. Soc.*, *77*, 437–471, 1996.

Karoly, D. J., Southern hemisphere circulation features associated with El Niño–Southern Oscillation events, *J. Clim.*, *2*, 1239–1252, 1989.

Kaylor, R. E., Filtering and decimation of digital time series, *Tech. Rep. Note BN 850*, Univ. of Md., College Park, 1977.

Meehl, G. A., The annual cycle and interannual variability in the tropical Pacific and Indian Ocean regions, *Mon. Weather Rev.*, *115*, 27–50, 1987.

Murphy, E. J., A. Clarke, C. Symon, and J. Priddle, Temporal variation in Antarctic sea-ice: Analysis of a long term fast-ice record from the South Orkney Islands, *Deep Sea Res., Part I*, *42*, 1045–1062, 1995.

Orsi, A. H., T. Whitworth III, and W. D. Nowlin Jr., On the meridional extent and fronts of the Antarctic Circumpolar Current, *Deep Sea Res., Part I*, *42*, 641–673, 1995.

Philander, S. G. H., *El Niño, La Niña and the Southern Oscillation*, 293 pp., Academic, San Diego, Calif., 1990.

Preisendorfer, R. W., *Principal Component Analysis in Meteorology and Oceanography*, Elsevier, New York, 1988.

Qiu, B., and F.-F. Jin, Antarctic circumpolar waves: An indication of ocean-atmosphere coupling in the extratropics, *Geophys. Res. Lett.*, *24*, 2585–2588, 1997.

Rasmusson, E. M., Observational aspects of ENSO cycle teleconnections, in *Teleconnections Linking Worldwide Climate Anomalies*, edited by M. H. Glantz, R. W. Katz, and N. Nicholls, pp. 309–343, Cambridge Univ. Press, New York, 1991.

Rasmusson, E. M., and K. Mo, Linkages between 200-mb tropical and extratropical circulation anomalies during the 1986–1989 ENSO cycle, *J. Clim.*, *6*, 595–616, 1993.

Reid, J. L., On the total geostrophic circulation of the South Pacific Ocean: Flow patterns, tracers and transports, *Prog. Oceanogr.*, *16*, 1–61, 1986.

Reid, J. L., On the total geostrophic circulation of the South Atlantic Ocean: Flow patterns, tracers and transports, *Prog. Oceanogr.*, *23*, 149–244, 1989.

Reynolds, R. W., A real-time global sea surface temperature analysis, *J. Clim.*, *1*, 75–86, 1988.

Reynolds, R. W., and D. C. Marisco, An improved real-time global sea surface temperature analysis, *J. Clim.*, *6*, 114–119, 1993.

Reynolds, R. W., and T. M. Smith, Improved global sea surface temperature analyses using optimum interpolation, *J. Clim.*, *7*, 929–948, 1994.

Sardeshmukh, P. D., and B. J. Hoskins, The generation of global rotational flow by idealized tropical divergence, *J. Atmos. Sci.*, *45*, 1228–1251, 1988.

Savage, M. L., C. R. Stearns, and G. A. Weidner, The Southern

Oscillation signal in Antarctica, in *Second Conference on Polar Meteorology and Oceanography*, pp. 141–144, Am. Meteorol. Soc., Boston, Mass., 1988.

Simmonds, I., and T. H. Jacka, Relationships between the interannual variability of Antarctic sea ice and the Southern Oscillation, *J. Clim.*, *8*, 637–647, 1995.

Sinclair, M. R., and X. Cong, Polar airstream cyclogenesis in the Australasian region: A composite study using ECMWF analyses, *Mon. Weather Rev.*, *120*, 1950–1972, 1992.

Smith, S. R., and C. R. Stearns, Antarctic climate anomalies surrounding the minimum in the Southern Oscillation Index, in *Antarctic Meteorology and Climatology: Studies Based on Automatic Weather Stations*, *Antarct. Res. Ser.*, vol. 61, edited by D. H. Bromwich and C. R. Stearns, pp. 149–174, AGU, Washington, D. C., 1993.

Sprintall, J., and D. Roemmich, Regional climate variability and ocean heat transport in the southwest Pacific Ocean, *J. Geophys. Res.*, *100*, 15,865–15,871, 1995.

Stramma, L., R. G. Peterson, and M. Tomczak, The South Pacific Current, *J. Phys. Oceanogr.*, *25*, 77–91, 1995.

Stricherz, J. N., D. M. Legler, and J. J. O'Brien, Atlas of Florida State University Indian Ocean winds for TOGA 1970–1985, Mesoscale Air-Sea Interaction Group technical report, 215 pp., Fla. State Univ., Tallahassee, 1993.

Tomczak, M., and J. S. Godfrey, *Regional Oceanography: An Introduction*, 422 pp., Pergamon, Tarrytown, N. Y., 1994.

Tourre, Y. M., and W. B. White, ENSO signals in global upper-ocean temperature, *J. Phys. Oceanogr.*, *25*, 1317–1332, 1995.

Tourre, Y. M., and W. B. White, Evolution of the ENSO signal over the Indo-Pacific domain, *J. Phys. Oceanogr.*, *27*, 683–696, 1997.

Trenberth, K. E., A quasi-biennial standing wave in the southern hemisphere and interrelations with sea surface temperature, *Q. J. R. Meteorol. Soc.*, *101*, 55–74, 1975.

Trenberth, K. E., General characteristics of El Niño-Southern Oscillation, in *Teleconnections Linking Worldwide Climate Anomalies*, edited by M. H. Glantz, R. W. Katz, and N. Nicholls, pp. 13–42, Cambridge Univ. Press, New York, 1991.

Trenberth, K. E., and T. J. Hoar, The 1990–1995 El Niño-Southern Oscillation event: Longest on record, *Geophys. Res. Lett.*, *23*, 57–60, 1996.

Tribbia, J. J., The rudimentary theory of atmospheric teleconnections associated with ENSO, in *Teleconnections Linking Worldwide Climate Anomalies*, edited by M. H. Glantz, R. W. Katz, and N. Nicholls, pp. 285–308, Cambridge Univ. Press, New York, 1991.

van Loon, H., and D. J. Shea, The Southern Oscillation, IV, The precursors south of 15°S to the extremes of the oscillation, *Mon. Weather Rev.*, *113*, 2063–2074, 1985.

van Loon, H., and D. J. Shea, The Southern Oscillation, VI, Anomalies of sea level pressure on the southern hemisphere and of Pacific sea surface temperature during the development of a warm event, *Mon. Weather Rev.*, *115*, 370–379, 1987.

Wang, B., Interdecadal changes in El Niño onset in the last four decades, *J. Clim.*, *8*, 267–285, 1995.

White, W. B., and R. G. Peterson, An Antarctic circumpolar wave in surface pressure, wind, temperature and sea-ice extent, *Nature*, *380*, 699–702, 1996.

White, W. B., and N. J. Cherry, Influence of the Antarctic Circumpolar Wave upon New Zealand temperature and precipitation during autumn-winter, *J. Clim.*, in press, 1998.

White, W. B., S.-C. Chen, and R. G. Peterson, The Antarctic Circumpolar Wave: A beta-effect in ocean-atmosphere coupling over the Southern Ocean, *J. Phys. Oceanogr.*, in press, 1998.

Wooster, W. S., and D. L. Fluharty (Eds.), *El Niño North. Niño Effects in the Eastern Subarctic Pacific Ocean*, 312 pp., Wash. Sea Grant Program, Univ. of Wash., Seattle, 1985.

Wyrtki, K., *Oceanographic Atlas of the International Indian Ocean Expedition*, 531 pp., Natl. Sci. Found., Washington, D. C., 1971.

Zwally, H. J., C. L. Parkinson, and J. C. Comiso, Variability of Antarctic sea ice and changes in carbon dioxide, *Science*, *220*, 1005–1012, 1983.

R. G. Peterson and W. B. White, Scripps Institution of Oceanography, University of California, San Diego, UCSD Mail Code 0230, La Jolla, CA 92093-0230. (e-mail: rpeterson@ucsd.edu; wbwhite@ucsd.edu)

(Received April 28, 1997; revised April 23, 1998;
accepted May 21, 1998.)